Structure and Orbital Angular Momentum of Singular Array of Gaussian Beams

A. Volyar, V. Shvedov, Ya. Izdebskaya, T. Fadeyeva and A. Rubass

Physics Department, Taurida National V. Vernandsky University, 4 Vernadsky Ave., 95007 Simferopol, Crimea, Ukraine e-mail: volyar@ccssu.crimea.ua

Received: 04.02.2006
After revision: 05.05.2006

Abstract

We consider theoretically and experimentally the structure and the orbital angular momentum (OAM) of the beam array consisting of aggregate of coherent fundamental Gaussian beams, whose axes are located on the surface of hyperboloid of revolution. An intrinsic characteristic of such the beam system is its OAM that cannot be eliminated by whatever transformations of the reference frame. This construction of the array enables one to change the OAM from zero up to very large values.

Key words: singular beams, optical vortices

PACS: 41.85.Ja, 41.85.Ct

1. Introduction

Singular laser arrays are a subject of a rapt attention because of their unique properties for trapping and transportation of microparticles [1] and other applications in both linear and nonlinear optics [2]. The most attractive feature of field structures in the singular laser arrays is an angular momentum that can be separated, in accordance with Allen et al. [3], into a spin angular momentum and an orbital angular momentum (OAM) for paraxial light beams. Manipulating topological charges of vortices and a circular polarization of the beam, we can create a field structure either with a double angular momentum or none momentum at all [3]. When the paraxial beam is linearly polarized, we can manage the OAM only.

A combination of laser beams (called as a beam array), whose axes are displaced with respect to the optical axis, has been earlier shown to enable creating a high-quality focal spot for medical and technical applications [4-6] after focusing with a lens system.

Experimental studies of similar beam arrays generated with a staircase mask [7] and a wedge stack [8] illustrate good singular properties of such systems. On the other hand, the authors of the study [9] have drawn attention to the fact that a misaligned single Gaussian beam (which is displaced and tilted with respect to some axis) possesses an OAM, whose value might be easily changed. At the same time, it is evident that the mentioned OAM could be eliminated by appropriate transformations of a frame of reference. We have supposed that a symmetric system of such misaligned beams could possess a number of novel intrinsic properties that are not inherent to separate singular beams.

The aim of the present work is to study a structure and OAM of misaligned beams, the axes of which are located on the surface of hyperboloid of revolution.

2. Field Structure of the Array

In order to make up the above beam system, we set the waist centres of the fundamental

Gaussian beams at the vertices of a regular polygon at the plane $z=0$ and at the distance r_0 from the origin O. The axes of all the beams are parallel to z axis of the initial reference frame $\{x,y,z\}$. Now all the beam axes lie at the cylindrical surface. Let we place the origin O' of a new frame of reference $\{x',y',z'\}$ at the n-th vertex of the polygon in such a way that the z' axis remains parallel to the generatrix of the cylinder, while the x' axis is rotated by the angle φ_n relative to the initial x axis. Then we tilt the $\{x',y',z'\}$ frame to the x' axis by an angle α (see Fig. 1), thus forming the reference frame $\{x_n,y_n,z_n\}$ associated with the n-th beam of the array. Having performed such the operations with all the beams, we create a light array with the beam axes laid on the surface of a hyperboloid of revolution. We will put that all the beams have the same waist radius ρ at the plane $z=0$.

In real beam systems, the angle α is very small ($\alpha \propto 10^{-2} \div 10^{-4}$ rad), so that $\sin\alpha \approx \alpha$. It is suitable to express the coordinates $\{x_n, y_n, z_n\}$ in terms of cylindrical coordinates $\{r,\varphi, z\}$ ($x=r\cos\varphi$ and $y=r\sin\varphi$). Then a given point A (see Fig. 1) has the coordinates

$$\begin{aligned} x_n &= r\cos(\varphi-\varphi_n)-r_0 \\ y_n &= r\sin(\varphi-\varphi_n)-\alpha z, \\ z_n &= \alpha r\sin(\varphi-\varphi_n)+z \end{aligned} \qquad (1)$$

while the radial position of this point is characterized by the radius $r_n^2 = x_n^2 + y_n^2$:

$$r_n^2 = \bar{r}^2 - 2r r_0\cos\vartheta_n - 2\alpha r z\sin\vartheta_n, \qquad (2)$$

where $\vartheta_n = \varphi - \varphi_n$ and $\bar{r}^2 = r^2 + r_0^2$.

Since the waist centres of the beams are lodged at the vertices of a regular polygon, the azimuthal coordinate of the n-th vertex is $\varphi_n = n\,2\pi/N$, with N standing for the number of vertices in the polygon (i.e., the number of beams in the array), whereas the index of each beam is $n=1,2,...N$. Let each beam have the initial phase $\Delta_n = \varphi_n l = \left(n\frac{2\pi}{N}\right)l$, ($l$=0, ±1, ±2,…, where l is a specific number of singular arrays). It means that each beam in the array gets the only additional phase at the $z=0$ plane, whose magnitude depends both on the beam position (the index n) and the initial conditions assigned by experimentalist (the index l), i.e. the phase Δ_n characterizes a phase matching in the array. For example, if the array has $N=3$ beams and $l=1$, then the full phase variation after going around the array axis z at some array cross-section is equal to 2π. This is an evidence of the fact that the array can potentially carry optical vortex with the topological charge equal to $+1$. On the other hand, the index -1 corresponds to a possible vortex with the topological charge equal to -1. The value $l=0$ is then associated with a topologically neutral beam array. However, as we will see later on, the value $l\neq 0$ is not a sufficient condition for arising the only vortex in the array.

Here we consider a scalar case of wave

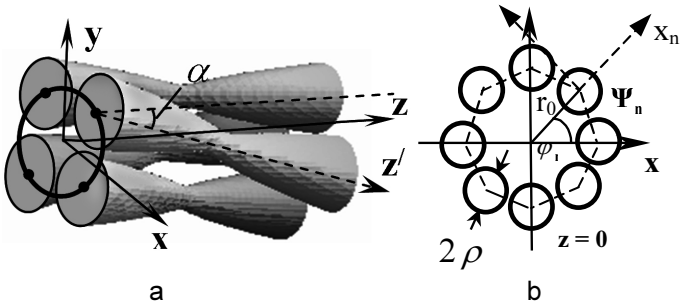

a b

Fig. 1 Sketch of singular beam array containing Gaussian beams in free space (a) and its cross-section by the plane z=0 (b).

propagation. Besides, we focus our attention on a paraxial approximation of the wave process. Then the transverse electric ($\mathbf{E}_t$) and magnetic ($\mathbf{H}_t$) vectors of the beam field may be expressed in terms of one scalar wave function Ψ_n, so that $\mathbf{E}_t(r,\varphi,z)=\mathbf{e}_t\,\Psi_n(r,\varphi,z)$ and $\mathbf{H}_t(r,\varphi,z)=\mathbf{h}_t\,\Psi_n(r,\varphi,z)$, where $\mathbf{e}_t$ and $\mathbf{h}_t$ are constant vectors. The wave function Ψ_n of the *n*-th fundamental Gaussian beam in the frame of reference $\{x_n, y_n, z_n\}$ is

$$\Psi_n=\frac{1}{Z_n}\exp\left\{-i\,k\,\frac{r_n^2}{2Z_n}\right\}\exp\left[i\left(k\,z_n-\Delta_n\right)\right], \quad (3)$$

where $Z_n=z_n+i\,z_0$, $z_0=k\rho^2/2$, and k is the wave number.

Now the wave function of the beam combination is

$$\Psi=\sum_{n=1}^{N}\Psi_n. \quad (4)$$

The expression (3) in common with Eq. (4) enable us to perform computer simulations of the wave structure. However, these expressions do not permit one analyzing theoretically the array behaviour and calculating its OAM. On the other hand, we could make use of the results [9] and expand the wave function (3) into a uniform series on Bessel functions. However, the obtained expression would consist of a product of two asymptotic series and any practical calculations employing them would be too difficult. Instead we will do the following. Since in our consideration α is a small angle, we could suppose, to a high enough degree of accuracy, that $1/Z_n\approx 1/Z$ ($Z=z+i\,z_0$). Using Eqs. (2) and (3), we can rewrite Eq. (4) as

$$\Psi=\Psi_0\sum_{n=1}^{N}\exp\left(A\exp(i\vartheta_n)+B\exp(-i\vartheta_n)\right)\exp(il\varphi_n)., \quad (5)$$

where $\Psi_0=\exp\left(-R^2+ikz\right)/Z$ $R^2=ik\bar{r}^2/2Z$,

$A=-i\frac{z_0}{Z}(\Re+\Xi)\frac{r}{\rho}$, $B=-i\frac{z_0}{Z}(\Re-\Xi)\frac{r}{\rho}$, and $\Re=r_0/\rho$, $\Xi=\alpha/\alpha_{diff}$, where $\alpha_{diff}=2/(k\rho)$ is the divergence angle of the Gaussian beam. Besides, we have $\vartheta_n=\varphi-\varphi_n$.

Making use of the series

$$\exp(x)=\sum_{j=0}^{\infty}\frac{x^j}{j!}, \quad (5a)$$

$$(x+y)^j=\sum_{p=0}^{j}\binom{j}{p}x^p y^{j-p} \quad (5b)$$

in Eq. (5), one obtains the expression

$$\Psi=\Psi_0\sum_{j=0}^{\infty}\frac{1}{j!}\sum_{p=0}^{j}\binom{j}{p}A^{j-p}B^p\exp\left[i(j-2p)\varphi\right]\sum_{n=1}^{N}\exp\left[i(j-2p+l)\varphi_n\right]. \quad (5c)$$

The third sum in Eq. (5c) represents a geometric series

$$\sum_{n=1}^{N}\exp\left[i(j-2p+l)\left(n\frac{2\pi}{N}\right)\right]=\begin{cases}N, & \text{if } j-2p+l=mN,\ m=0,\pm1,\pm2,\ldots\\ 0, & \text{elsewhere}\end{cases} \quad (6)$$

Consequently, we find that

$$\Psi=\Psi_0 N\sum_{m=-\infty}^{\infty}\exp(i\,L_m\varphi)\times\sum_{q=0}^{\infty}\frac{1}{k!}\binom{q}{\frac{q-L_m}{2}}A^{\frac{q+L_m}{2}}B^{\frac{q-L_m}{2}}, \quad (7)$$

where $L_m=mN-l$ and $l<N$. The value $\frac{(q-L_m)}{2}$ in the binomial coefficient of Eq. (7) must be an integer. This requirement results in two possible types of series in Eq. (7) for odd and even integers in the binomial coefficient:

$$\sum_{q=0}^{\infty}\frac{1}{(2q)!}\binom{2q}{q+s}x^{2q}=I_{2s}(2x), \quad (8)$$

$$\sum_{q=0}^{\infty}\frac{1}{(2q+1)!}\binom{2q+1}{q+s}x^{\frac{2q+1}{2}}=I_{2s-1}\left(2\sqrt{x}\right), \quad (9)$$

where $I_v(x)$ denotes the modified Bessel function and $s=0,\pm1,\pm2,\ldots$. We finally obtain the wave function of the array in the form

$$\Psi=\Psi_0 N\sum_{m=-\infty}^{\infty}\left(\frac{A}{B}\right)^{\frac{mN-l}{2}}I_{mN-l}\left(2\sqrt{AB}\right) \quad (10)$$
$$\times\exp\left[i\left(mN-l\right)\varphi\right].$$

Besides, we can express the variable AB at the z=0 plane through the dimensionless natural parameters $\Re$ and Ξ:

$$AB=\frac{r^2\left(\Xi^2-\Re^2\right)}{\rho^2} \text{ and } \frac{A}{B}=\frac{\Re+\Xi}{\Re-\Xi}. \quad (11)$$

The expression (11) possesses a number of important properties. First of all, we can restrict ourselves only to two terms in Eq. (7) with $m=0$, $m=+1$ for $l>0$ and $m=-1$ for $l<0$ ($|l|<N$), provided that the parameters $\Re$ and Ξ are small ($\Re,\Xi<<1$). For example, in a simple case of $N=2$ and $l=1$, we find from Eq. (11) for the central vortex that

$$\Psi\approx 2I_1\left(2\sqrt{AB}\right)\left[\sqrt{\frac{B}{A}}\exp\left(-i\varphi\right)+\right.$$
$$\left.+\sqrt{\frac{A}{B}}\exp\left(i\varphi\right)\right]\exp\left(-ik\frac{r^2+r_0^2}{2Z}\right)\frac{\exp\left(ikz\right)}{Z}. \quad (12)$$

This wave function describes the wave propagation of ordinary Bessel-Gaussian beam bearing two optical vortices with the topological charges $l=-1$ and $l=+1$ and different weights (a so-called anisotropic vortex). At the same time, a pure optical vortex appears at $z=0$ plane if we have $\Re=\Xi$. However, as the array propagates along z axis, the value $A'B'\neq 0$ and the vortex structure is distorted. On the other hand, the array carries a pure edge dislocation along the z axis, if the angle α=0 and $\Psi\propto r\cos\varphi$. Moreover, we may describe the array propagation in frame of the Bessel-Gaussian beam approximation in the more general cases $|l|>1$ and $N>2$. However, large values of the parameters $\Re$ and Ξ cause us to take into account additional terms in the series. So, variations in the angle α and the displacement r_0 result in arising a vortex chain in case of two beams in the array (see the state **{2, 1}** in Fig. 2) or a vortex net for higher-order arrays (see the rest of the states displayed in Fig. 2). The states of the array are completely characterized by means of the two numbers **{N, *l*}** and the two dimensionless parameters $\{\Re,\Xi\}$. Fig. 2 illustrates the structure of intensity distribution of the array in different states **{N, *l* }**.

3. Orbital Angular Momentum

In order to find the OAM, we use the expression [10],

$$L_z=i\left\langle\Psi\left|\frac{\partial}{\partial\varphi}\right|\Psi\right\rangle=i\int_0^{2\pi}d\varphi\int_0^{\infty}r\,\Psi^*\partial_\varphi\Psi\,dr. \quad (13)$$

The magnitude of the OAM is (see Appendix A) as follows:

$$L_z=\left\{l\sum_{m=-\infty}^{\infty}\aleph^{mN-l}I_{mN-l}\left(2\Theta\right)\right.$$
$$\left.-N\sum_{m=-\infty}^{\infty}m\,\aleph^{mN-l}I_{mN-l}\left(2\Theta\right)\right\}\exp\left(\Theta\right), \quad (14)$$

where

$$\Theta=\left(\Xi^2-\Re^2\right),\ \aleph=\left(\Xi-\Re\right)/\left(\Xi+\Re\right) \quad (15)$$

and $l\geq 0$.

First of all, it is necessary to note that the OAM in Eq. (14) does not depend on the longitudinal coordinate z and so it is an invariant of the array [3, 11]. Besides, the presence of two variables Ξ and $\Re$ (see Eq. (15)) supposes a complete behaviour of the OAM under variations of the angle α and the displacement r_0 in the array. At the same time, we can conditionally speak about two processes connected with a destructive interference and array geometry that contribute to the OAM. It is these complete variables that evidence two competitive processes. The first of them is connected with a destructive interference between the phase-matched beams, which

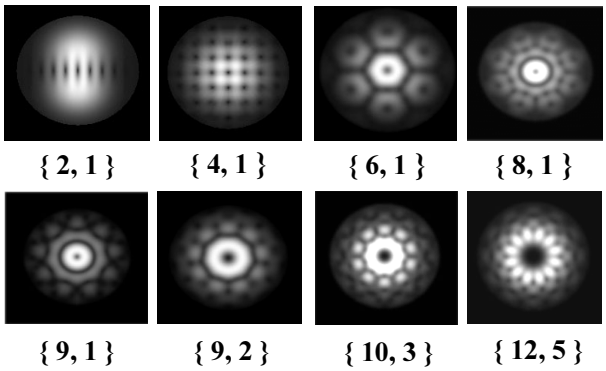

Fig. 2. Structure of intensity distribution of the array in different states **{N, *l*}** for $\Re = 0.2$ and $\Xi = 0.1$.

results in creating optical vortices, while the second process is associated with the geometry of the array. It is a symmetrical system of skew beams that has created an additional OAM inherent even to incoherent beam system.

Fig. 3 illustrates variations of the normalized OAM $L_z / L_{\max}$ dependent upon the dimensionless displacement $\Re$ (Fig. 3a) and the angle Ξ (Fig. 3b). The angular momentum $L_z(\Re)$ increases at first, passes through the maximum and then begins to decrease. Further behaviour of the OAM depends on the magnitude and sign of the angle Ξ. Zero angle Ξ predetermines a fast reduction of OAM down to zero, when the displacement $\Re$ increases. Indeed, as the beams are removed far from the array axis, the contribution of destructive interference decreases and the OAM tends to zero. However, decreasing behaviour of the AOM turns into growth of its modulus, when the angle Ξ differs from zero.

It is important to stress an interesting trait of the phase-matched beam array. So, the angular momentum of a misaligned beam [9] can be eliminated if the origin of the reference frame coincides with the beam axis ($\Re = 0$), though $\Xi \neq 0$. Moreover, the OAM of an array of equal-phase beams with a common origin is also zero for any angles Ξ. In this case the geometrical contribution to the OAM vanishes. A completely different type of behaviour occurs for the phase-matched array. Fig. 3b shows that the OAM in such the beam array (with the beams coincident at $z = 0$ plane) increases as the angle Ξ changes. A central zero in the intensity distribution presented in Fig. 4a and a nearly helical shape of a wave front (Fig. 4b) point out that the destructive interference here forms an optical vortex at the array axis.

For practical estimations, it would be very suitable to use the OAM per photon [3] defined as a ratio L_z / I, where I stands for the beam intensity. In our calculations we employ the magnitude $\langle \Psi | \Psi \rangle$ being proportional to the

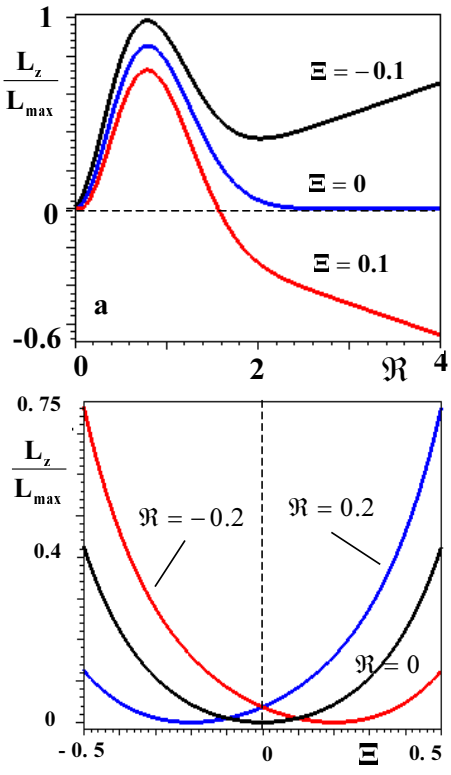

Fig. 3. Variations of normalized OAM $\frac{L_z}{L_{\max}}$ as a function of dimensionless displacement $\Re$ (a) and angle Ξ (b) in the array for the state {3, 1}.

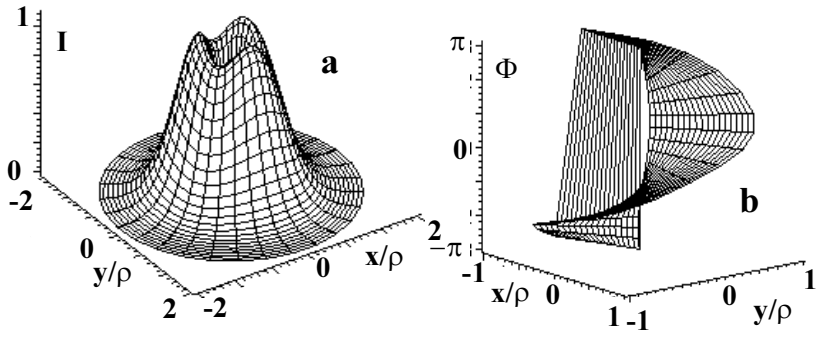

Fig. 4. Intensity distribution I (a) and wave front surface (b) for the {3, 1} state of the array at z=0, $\Re = 0$ and $\Xi = 0.1$.

intensity, so that the magnitude $\eta = L_z / \langle \Psi | \Psi \rangle$ is the specific OAM (i.e., the OAM per photon for a given frequency ω). Using Eqs. (13) and (14), we obtain

$$\eta = \frac{L_z}{\langle \Psi | \Psi \rangle} = l - \frac{N \sum_{m=-\infty}^{\infty} m \, \aleph^{mN-l} I_{mN-l}(2\Theta)}{\sum_{m=-\infty}^{\infty} \aleph^{mN-l} I_{mN-l}(2\Theta)}. \quad (15)$$

This equation enables us to simplify evaluation of the specific OAM η under the condition of $\Theta << 1$. In Appendix B, we show that for this case

$$\eta \approx l - N \frac{(\Xi - \Re)^{2(N-l)}}{(\Xi + \Re)^{2l} + (\Xi - \Re)^{2(N-l)}}. \quad (16)$$

Thus, Eq. (16) may be rewritten for very small displacements $\Re$ and angles Ξ as

$$\eta_0 = \lim_{\Re, \Xi \to 0} \eta = \begin{cases} 0, & N = 2l \text{ and } N = l \\ l, & N > 2l \\ l - N, & N < 2l \end{cases}. \quad (17)$$

One should bear in mind that the total intensity of the phase-matched array is equal to zero if $\Re = \Xi = 0$, i.e. $\langle \Psi | \Psi \rangle_{\Re=0, \Xi=0} = 0$ and $L_z(\Re = 0, \Xi = 0) = 0$, too. Consequently, the specific OAM is uncertain at this point. But any slight (as small as we wish) angular or linear displacement of the beams takes this uncertainty away. Thus, Eq. (16) takes place for all $|\Xi|, |\Re| << 1$, except for the point $\Re = \Xi = 0$.

Besides, Eqs. (14) and (16) have been derived from Eqs. (10) and (13), provided that $l < N$ (see Eqs. (6) and (7)). The condition $l \geq N$ corresponds to the beams with equal initial phases. As a consequence, we can expand Eq. (17) to the case of $\eta_0 = 0$, if only $l \geq N$.

The expressions (16) and (17) show that the beam array with even number of beams has a zero OAM (if Ξ=0) for any linear displacement $\Re$, if $N = 2l$. At the same time, phase-matched arrays with an odd number of beams always carry OAM.

The initial OAM of the array caused by destructive interference can be completely suppressed by picking up the appropriate angle Ξ=0 or the displacement $\Re$ (see, e.g., Fig. 3a and b). This effect manifests itself most distinctly in the dependence $\eta(\Xi)$ for the array state **{3, 1}** shown in Fig. 5a. The specific OAM is unit ($\eta = 1$) for the angle Ξ=0. Fig. 5b illustrates a nearly ideal optical vortex typical for this case. With decreasing angle Ξ, the specific OAM decreases, too. It crosses Ξ axis at the point $\Xi \approx 0.12$. Although the array does not carry OAM now, the optical vortex is cited at the array axis (see Fig. 5c). However, the structure of the beam is distorted. Additional optical vortices with the opposite topological charges appear at the beam edges.

To calculate the angle Ξ_0 that corresponds to zero angular momentum of the array, it is necessary to equate the second term in Eq. (16) to the first one. After simple mathematical transformations we find

$$\Xi_0 = \frac{1}{2l} \frac{(N-l)\Re - l\Re^{2(N-2l)+1}}{N + 1 - (N-l)\Re^{2(N-2l)}}, \quad (18)$$

where we have supposed that $\Re >> \Xi$ and employed Eq. (5b). This angle characterizes the point where the two competitive processes (those related to the destructive interference and the array geometry) counterbalance each other.

Variations of the angle Ξ in the area $-1 < \Xi < 0$ for $l > 0$ (or in the area $0 < \Xi < 1$ for $l < 0$) are accompanied by drastic variations of the specific OAM η. However, a subsequent decrease (or increase) in the angle Ξ is associated with a monotonous decrease (or increase) in the angular momentum. In particular, the linear dependence between the specific OAM η and the parameters Ξ and $\Re$ becomes apparent for $\Re >> 1$:

$$\eta \approx 2\Re\Xi = k r_0 \alpha . \qquad (19)$$

It is in this area that the destructive interference vanishes (see Appendix C). This expression shows also that we can reach rather high OAM values with appropriate manipulations of the displacement $\Re$ and the angle Ξ. Besides, *such the OAM inheres in any symmetric compositions of Gaussian beams and cannot be eliminated whatever transformations of the frame of reference are performed.*

4. Optical Wedge as a Device for Generating Singular Beam Arrays

The method of the amplitude masks and the computer-generated hologram technique are typical methods for generating equal-phase beam arrays (see, e.g., [1]). On the other hand, we have recently illustrated [8] a capability of wedge stacks for generating phase-matched

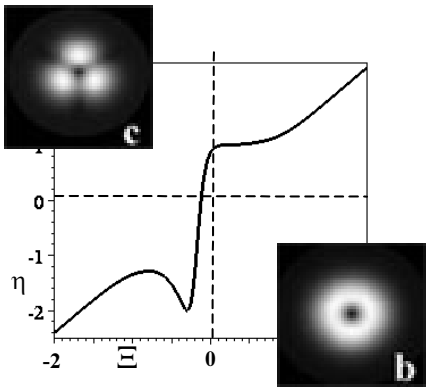

Fig. 5. Dependence of angular momentum η on dimensionless parameter Ξ for the vortex-bearing array with a zero OAM: **{3, 1}** and $\Re = 0.1$.

arrays bearing high-order optical vortices. Such singular arrays have also turned out to be stable under focusing with lens systems [12]. The beam array has been shaped due to diffraction of beam at the edge of each wedge in the stack. Here we will demonstrate experimentally one more property of the wedge surface (in contrast to the wedge edge) that consists in possibility for creating singular arrays of a lower order for the case of reflected light.

We have made use of a thin dielectric wedge with a small wedge angle θ and a refractive index n. Let a fundamental Gaussian beam fall onto the wedge in arbitrary way relative to the wedge verges. In a general case, the beam axis in the wedge is characterized by the two angles β and γ for the two projections on the *zx* and *zy* planes (see Fig. 6). The combinations of those beams reflected by the wedge are displaced by the distance r_0 and tilted at the angle α to each other.

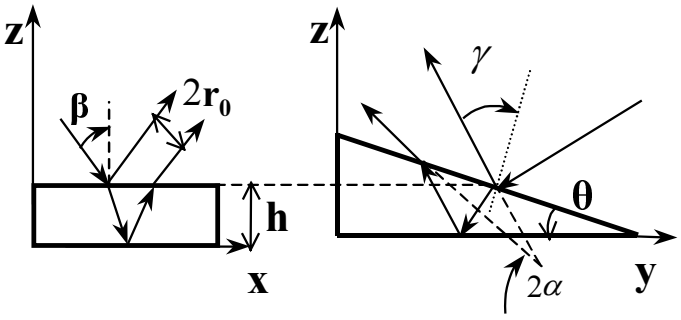

Fig. 6. Projections of optic axis of the Gaussian beam incident oblique upon the wedge.

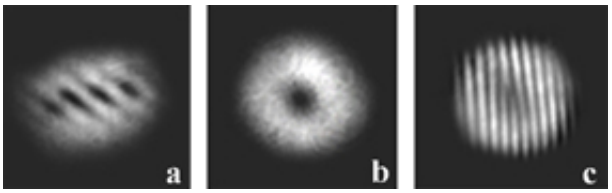

Fig. 7. Experimental intensity distribution in the array generated by the wedge: (a) the vortex chain ($\alpha \approx 10^{-2}$ rad and $r_0 \approx 50$ μm); (b) and (c) single-charged vortex and its interferential pattern ($\alpha \approx 4\times10^{-3}$ rad and $r_0 \approx 25$ μm).

This means that the axes of the two reflected beams are not crossed. A simple geometrical consideration gives basic relationships between the wedge parameters, the beam displacement $2r_0$ and the angle 2α in the following form:

$$r_0 = \frac{1}{2}\frac{h\sin 2\beta}{\sqrt{n^2 - \sin^2\beta}},\ \alpha \approx (n-1)\frac{\theta}{2}. \qquad (20)$$

The phase shift Δ between the beams can be manipulated by changing the beam incidence point on the upper wedge surface and the angles β and γ. Besides, the second beam gets the additional phase π at the expense of reflection by the lower wedge surface. As a consequence, they form elementary beam array with $N = 2$ and $l = 1$. In the experiment we have employed a glass wedge with the refractive index n=1.5. The wedge angle varies over the wedge surface within the interval of $\theta \approx (2 \div 9)\cdot 10^{-3}$ rad.

The wedge has been illuminated with the radiation of He-Ne laser ($\lambda = 0.6328\,\mu$m).The wedge thickness could be changed from 25 to 55 μm at the incidence point. Let the fundamental Gaussian beam with $\rho = 0.5$mm is focused by the lens ($f = 150$mm) onto the wedge surface. The beam waist at the focal plane is about $\rho = 50\,\mu$m. Two reflected beams form the array whose intensity distribution is detected by a CCD camera. In a general case, the destructive interference of skew beams forms a chain of optical vortices, whose structure is essentially distorted (see Fig. 7a and compare it with Fig. 2a). Any variations of the lens position and the positions of the beam waist at the wedge surface result in changing the vortex structure. The array with a single centred vortex is created in case when the waist of the initial beam is sited at the wedge surface (see Fig. 7b and c).

5. Conclusions

Thus, we have shown theoretically that a phase-matched composition of Gaussian beams, whose axes lie on the surface of hyperboloid of revolution, form a singular beam array that bears a net of optical vortices. The state of the array is defined by the two number **{N, *l*}** and the two dimensionless parameters: the angle Ξ and the displacement $\Re$. It is these four numbers that characterize the OAM of the array. We have revealed that there are two competitive processes inside the interval of parameters $\Re^2 \le \Xi^2$, which can form the array with a zero OAM that nevertheless bears an optical vortex. Moreover, the OAM of the array can unrestrictedly increase outside this interval. Let us also notice that the OAM of symmetric compositions of Gaussian beams cannot vanish after whatever transformations of a reference frame.

Furthermore, we have illustrated a simple experimental technique based on utilizing a dielectric wedge that enables us to generate low-order singular beam arrays.

Acknowledgements

The authors wish to express their gratitude to Dr. A. Desyatnikov (Australian National University, Canberra), Professor A. Bekshaev (Mechnicov National University, Odessa, Ukraine) and Dr. C. Alexeyev (Taurida National University, Simferopol, Ukraine) for valuable discussions.

Appendix A

At first we find the integral over azimuthal angle φ in Eq. (13), employing the integral

$$\int_0^{2\pi} \exp\{i(m-q)\varphi\}\, d\varphi = \begin{cases} 2\pi, & \text{if } m = q \\ 0, & \text{otherwise} \end{cases},$$

so that

$$L_z = -2\pi N^2 \exp\left(-\frac{r_0^2}{\rho^2}\right)\times$$
$$\times \sum_{m=-\infty}^{\infty} (mN-l)\left(\frac{A}{B}\right)^{mN-l} \times \qquad \text{(A1)}$$
$$\times \int_0^{\infty} r\, I_{mN-l}^2\left(2\sqrt{AB}\right)\exp\left(-\frac{r^2}{\rho^2}\right) dr$$

Then we have

$$\int_0^{\infty} x \exp\left(-p x^2\right) I_v(b x) I_v(c x) dx$$
$$= \frac{1}{2p}\exp\left(\frac{b^2+c^2}{4p}\right) I_v\left(\frac{bc}{2p}\right), \qquad \text{(A2)}$$

whence we find Eq. (14) provided that $a = b$ in Eq. (A2).

Appendix B

One can present the sum in the numerator of the second term in Eq. (16) in the form

$$S_1 = -\sum_{m=0}^{\infty} m\aleph^{-(mN+l)} I_{mN+l}(2\Theta)$$
$$+ \sum_{m=1}^{\infty} m\aleph^{mN-l} I_{mN-l}(2\Theta)$$
$$= -\sum_{m=0}^{\infty} m\aleph^{-(mN+l)} I_{mN+l}(2\Theta) \qquad \text{(A3)}$$
$$+ \sum_{m=0}^{\infty} (m+1)\aleph^{[(m+1)N-l]} I_{(m+1)N-l}(2\Theta)$$

Since $\Theta << 1$, we can use the approximation of modified Bessel function

$$I_{mN-l}(2\Theta) \approx \Theta^{|mN-l|} \qquad \text{(A4)}$$

and so obtain

$$S_1 \approx \sum_{m=0}^{\infty}\left\{-m(\Xi+\Re)^{2(mN+l)} + (m+1)(\Xi-\Re)^{2(mN-l)}\right\},$$

where $\frac{\Theta}{\aleph} = (\Xi+\Re)^2$ and $\Theta\aleph = (\Xi-\Re)^2$. The fist and the second terms in the last equation are geometric series:

$$\sum_{m=0}^{\infty} m x^{2N} = \frac{x^{2N}}{\left(x^{2N}-1\right)^2}, \qquad \text{(A5)}$$

$$\sum_{m=0}^{\infty} x^{2N} = -\frac{1}{x^{2N}-1}. \qquad \text{(A6)}$$

Thus, we have

$$S_1 \approx \left\{1-(\Xi+\Re)^{2N}\right\}^{-2}\left\{-(\Xi+\Re)^{2(N+l)}\right.$$
$$\left.+(\Xi-\Re)^{2(2N-l)}\right\} - \frac{(\Xi-\Re)^{2(N-l)}}{(\Xi-\Re)^{2N}-1}. \qquad \text{(A7)}$$

Similarly we find the sum in the denominator of the second term in Eq. (16):

$$S_2 \approx \frac{(\Xi+\Re)^{2l}}{1-(\Xi+\Re)^{2N}} + \frac{(\Xi-\Re)^{2l}}{1-(\Xi-\Re)^{2N}}. \qquad \text{(A8)}$$

Issuing from the assumption that $\Xi, \Re << 1$ and using Eqs. (A7), (A8) and (15), we finally arrive at Eq. (16).

Appendix C

The contribution of the destructive interference to shaping the phase-matched beam array becomes weaker as the distance between the beam axes increases, i.e. when $\Xi << 1, \Re >> 1$. Then it is sufficient to consider the OAM of a single misaligned beam, whereas the total OAM of the array is a sum of partial OAMs.

We put $N = 1$ and $l = 0$ in Eq. (15). Then the numerator and the denominator of the second term in Eq. (15) change respectively to the following forms:

$$S_1 = \sum_{m=-\infty}^{\infty} m\aleph^m I_m(2\Theta), \qquad \text{(A9)}$$

$$S_2 = \sum_{m=-\infty}^{\infty} \aleph^m I_m(2\Theta). \qquad \text{(A10)}$$

At the same time, the modified Bessel functions arise in the generating function relation [13]:

$$\exp\left\{\left(t+\frac{1}{t}\right)\frac{z}{2}\right\} = \sum_{m=-\infty}^{\infty} t^m I_m(z). \qquad \text{(A11)}$$

Thus, we obtain

$$S_2 = \exp\left(\Xi^2+\Re^2\right). \qquad \text{(A12)}$$

On the other hand, we have

$$\sum_{m=-\infty}^{\infty} m t^m I_m(z) =$$

$$= \frac{z}{2} \sum_{m=-\infty}^{\infty} t^m \left[I_{m-1}(z) - I_{m+1}(z) \right] = , \quad \text{(A13)}$$

$$= \frac{z}{2}\left(t - \frac{1}{t} \right) \exp\left\{ \left(t + \frac{1}{t} \right) \frac{z}{2} \right\}$$

where we have used the recurring relation for the modified Bessel functions:

$$I_m(z) = \frac{z}{2m} \left[I_{m-1}(z) - I_{m+1}(z) \right],$$

so that

$$S_1 = -2\Xi\Re \exp\left(\Xi^2 + \Re^2 \right). \quad \text{(A14)}$$

Substituting Eqs. (A12) and (A14) into Eq. (15), we get Eq. (19).

References

1. Bouchal Z. and Courtial J., J. Opt. Soc. Am. **A. 6.** (2004) 184.
2. Desyatnikov A.S., Denz C. and Kivshar Yu.S., Opt. Soc. Am. **A. 6.** (2004) 209; Desyatnikov A.S., Kivshar Yu.S. and Torner L. Progress in Optics (ed. E. Wolf) **47** (2005) 1.
3. Allen L., Paddget M. and Babiker B., Progress in Optics (ed. E. Wolf). **39** (1999) 291.
4. Baida Lii and Hong Ma. Opt. Comm. (2000) 178.
5. Engel E., Huse N., Klar T. and Hell S., Appl. Phys. **77** (2003) 11.
6. Bouchal Z., J. Opt. Soc. Am. A. **21** (2004) 1694.
7. Swartzlander G.A. and Schmit J., Phys. Rev. Lett. **93** (2004) 093901.
8. Izdebskaya Ya., Shvedov V. and Volyar A., Opt. Lett. **30** (2005) 2472.
9. Vasnetsov M., Pas'ko V. and Soskin M., New J. Phys. **7** (2005) 2.
10. Berry M., Proc. SPIE. **3487** (1998) 6.
11. Bekshaev A., Soskin M. and Vasnetsov M., Opt. Comm. **249** (2005) 367.
12. Izdebskaya Ya., Shvedov V. and Volyar A., Opt. Lett. **30** (2005) 2530.
13. Handbook of mathematical functions. Ed. M. Abramowitz and I. Stegun. National bureau of standards. Applied Mathematics series. **55** N.Y. 1964.